International Journal of Nanomedicine

Dovepress
open access to scientific and medical research

Open Access Full Text Article

ORIGINAL RESEARCH

# Tumor-Targeted cRGD-Coated Liposomes Encapsulating Optimized Synergistic Cepharanthine and IR783 for Chemotherapy and Photothermal Therapy

Yumei Wu[1–3,*], Chunhua Zeng[1–3,*], Jiajia Lv[1–3], Hongyu Li[1–3], Jie Gao[1–3], Zhidong Liu[4], Zeli Yuan[1–3]

[1]Key Laboratory of Basic Pharmacology of Ministry of Education and Joint International Research Laboratory of Ethnomedicine of Ministry of Education, Zunyi Medical University, Zunyi, 563000, People's Republic of China; [2]Key Laboratory of Biocatalysis & Chiral Drug Synthesis of Guizhou Province, School of Pharmacy, Zunyi Medical University, Zunyi, 563000, People's Republic of China; [3]Guizhou International Scientific and Technological Cooperation Base for Medical Photo-Theranostics Technology and Innovative Drug Development, Zunyi Medical University, Zunyi, 563000, People's Republic of China; [4]Engineering Research Center of Modern Chinese Medicine Discovery and Preparation Technique, Ministry of Education, Tianjin University of Traditional Chinese Medicine, Tianjin, 301617, People's Republic of China

*These authors contributed equally to this work

Correspondence: Zhidong Liu, Tianjin University of Traditional Chinese Medicine, No. 10 Poyanghu Road, Tianjin, Jinghai District, 301617, People's Republic of China, Email lonerliuzd@163.com; Zeli Yuan, Zunyi Medical University, Zunyi, 563000, People's Republic of China, Email zlyuan@zmu.edu.cn



**Background:** Combination therapy offers superior therapeutic results compared to monotherapy. However, the outcomes of combination therapy often fall short of expectations, mainly because of increased toxicity from drug interactions and challenges in achieving the desired spatial and temporal distribution of drug delivery. Optimizing synergistic drug combination ratios to ensure uniform targeting and distribution across space and time, particularly in vivo, is a significant challenge. In this study, cRGD-coated liposomes encapsulating optimized synergistic cepharanthine (CEP; a chemotherapy drug) and IR783 (a phototherapy agent) were developed for combined chemotherapy and photothermal therapy in vitro and in vivo.

**Methods:** An MTT assay was used to evaluate the combination index of CEP and IR783 in five cell lines. The cRGD-encapsulated liposomes were prepared via thin-film hydration, and unencapsulated liposomes served as controls for the loading of CEP and IR783. Fluorescence and photothermal imaging were used to assess the efficacy of CEP and IR783 encapsulated in liposomes at an optimal synergistic ratio, both in vitro and in vivo.

**Results:** The combination indices of CEP and IR783 were determined in five cell lines. As a proof-of-concept, the optimal synergistic ratio (1:2) of CEP to IR783 in 4T1 cells was evaluated in vitro and in vivo. The average diameter of the liposomes was approximately 100 nm. The liposomes effectively retained the encapsulated CEP and IR783 in vitro at the optimal synergistic molar ratio for over 7 d. In vivo fluorescence imaging revealed that the fluorescence signal from cRGD-CEP-IR783-Lip was detectable at the tumor site at 4 h post-injection and peaked at 8 h. In vivo photothermal imaging of tumor-bearing mice indicated an increase in tumor temperature by 32°C within 200 s. Concurrently, cRGD-CEP-IR783-Lip demonstrated a significant therapeutic effect and robust biosafety in the in vivo antitumor experiments.

**Conclusion:** The combination indices of CEP and IR783 were successfully determined in vitro in five cell lines. The cRGD-coated liposomes encapsulated CEP and IR783 at an optimal synergistic ratio, exhibiting enhanced antitumor effects and targeting upon application in vitro and in vivo. This study presents a novel concept and establishes a research framework for synergistic chemotherapy and phototherapy treatment.

**Keywords:** drug delivery, liposomes, synergistic effects, phototherapy

## Introduction

With the rapid development of treatment methodologies, various technologies pertaining to tumor therapy have undergone further development and practical implementation, encompassing conventional clinical treatment approaches, such

Received: 31 January 2024
Accepted: 1 June 2024
Published: 19 June 2024

**Graphical Abstract**

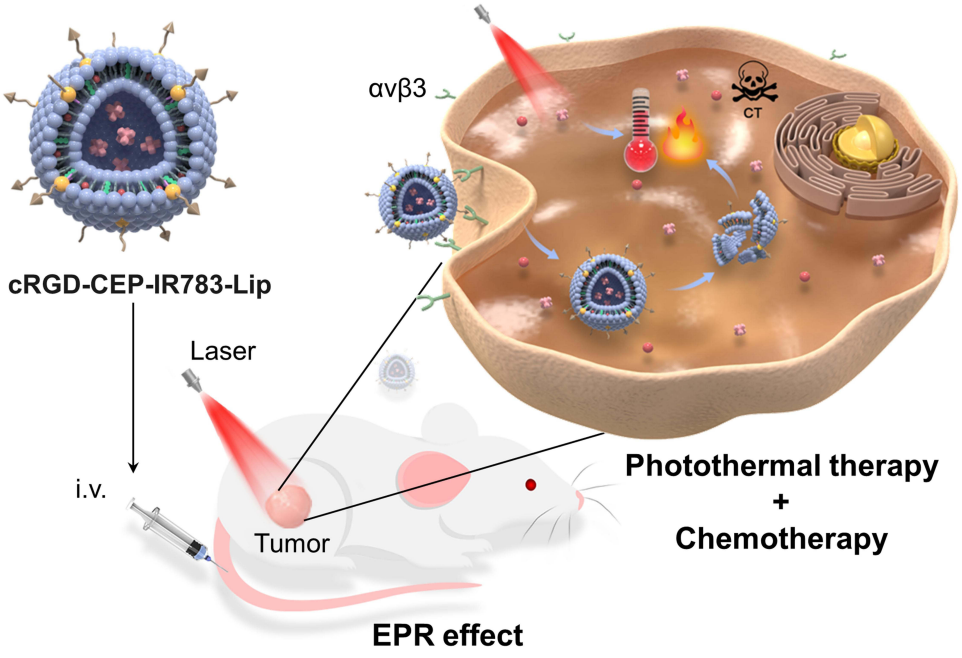


as chemotherapy, radiotherapy, and surgery, as well as innovative methods, such as photothermal therapy (PTT) and photodynamic therapy.[1,2] These multifaceted approaches have exhibited significant success in inhibiting tumor growth and prolonging patient survival. Nevertheless, both clinical observations and scientific investigations have revealed that single treatments often fail to completely prevent cancer recurrence. Several studies have indicated that this phenomenon can be attributed to the development of resistance in subpopulations of tumor cells within heterogeneous tumor tissues. This resistance makes them unresponsive to monotherapy, leading to the incomplete eradication of cancer cells and an increased risk of metastatic tumor formation.[3–5] In recent years, advances in cancer treatment have shifted the focus from monotherapy to combination therapy, involving the collaboration of two or more treatments to augment synergistic interactions. Combination therapy can potentially yield remarkable super-additive effects (1 + 1 > 2), improving effectiveness while minimizing toxicity.[6–8]

Consequently, identifying appropriate combination ratios and ensuring consistent spatiotemporal drug delivery have emerged as critical tasks. The traditional "cocktail" drug combination therapy represents significant progress in antitumor treatment. However, it is accompanied by unavoidable negative aspects owing to the intricate physiological conditions of the human body and the divergent pharmacokinetic processes of drugs.[9] To date, the integration of multiple therapeutic modalities using nanoplatforms has become a pivotal avenue for generating synergistic effects and minimizing toxicity, thus overcoming the limitations of monotherapy or "cocktail" drug combinations. Functionalized nanocarriers can serve as carriers of two or more therapeutic agents,[10] enabling co-delivery for synergistic treatment with distinct therapeutic modalities.[11] The dual-drug delivery system has become an important form of drug delivery in co-delivery formulations owing to its simple composition. Chen et al used exosomes co-encapsulated with galectin-9 siRNA and oxaliplatin for enhancing immunotherapy in cancer treatment.[12] Mukesh et al developed a cyclodextrin-conjugated nanoparticle co-encapsulated with rifampicin and levofloxacin to improve the treatment effect of tuberculosis.[13] Furthermore, nanocarriers can passively accumulate and persist at the tumor site owing to the enhanced permeability and retention (EPR) effect.[14–17] Additionally, these functionalized carriers can curtail uptake by the reticuloendothelial system.[18,19] Specifically, liposomes have proven to be efficacious in clinical applications as versatile nanocarriers, owing to their easy preparation, high biocompatibility, and ability to concurrently load and deliver drugs with diverse properties.[20] With the in-depth study of liposomes, dual-drug-loaded liposomes have received extensive attention

in clinical and exploratory experiments.[21] Vyxeos (CPX-351), a liposome-based formulation loaded with two drugs, cytarabine and daunorubicin, in a synergistic molar ratio (5:1), has received approval from the Food and Drug Administration for the treatment of high-risk acute myeloid leukemia.[22] Thus, encapsulating two or more diverse agents within liposomes emerges as a viable strategy that enhances the spatio-temporal consistency of drug delivery and facilitates synergistic treatment.

In this study, cepharanthine (CEP) and IR783 were co-loaded into liposomes as chemotherapeutic and photothermal agents, respectively, to examine their therapeutic efficacy at optimal synergistic ratios in vitro and in vivo. CEP, a natural small-molecule alkaloid extracted from *Stephania*, exhibits anticancer effects, including the inhibition of cell proliferation, promotion of apoptosis, and anti-angiogenesis effects.[23,24] IR783, a commercially available near-infrared phototherapy agent, demonstrates high fluorescence quantum yield and excellent phototherapy performance. Nevertheless, its rapid systemic clearance imposes limitations, leading to short retention at the tumor site.[25]

In this study, cRGD polypeptide-modified liposomes (cRGD-CEP-IR783-Lip) were designed and prepared to simultaneously deliver CEP and IR783 to the tumor in an optimal synergistic ratio (Scheme 1). Initially, the optimal synergistic ratio between CPE and IR783 was determined for five cancer cell lines (Scheme 1A). Subsequently, cRGD-modified liposomes were designed to improve tumor targeting by binding to the overexpressed αvβ3 integrin on the

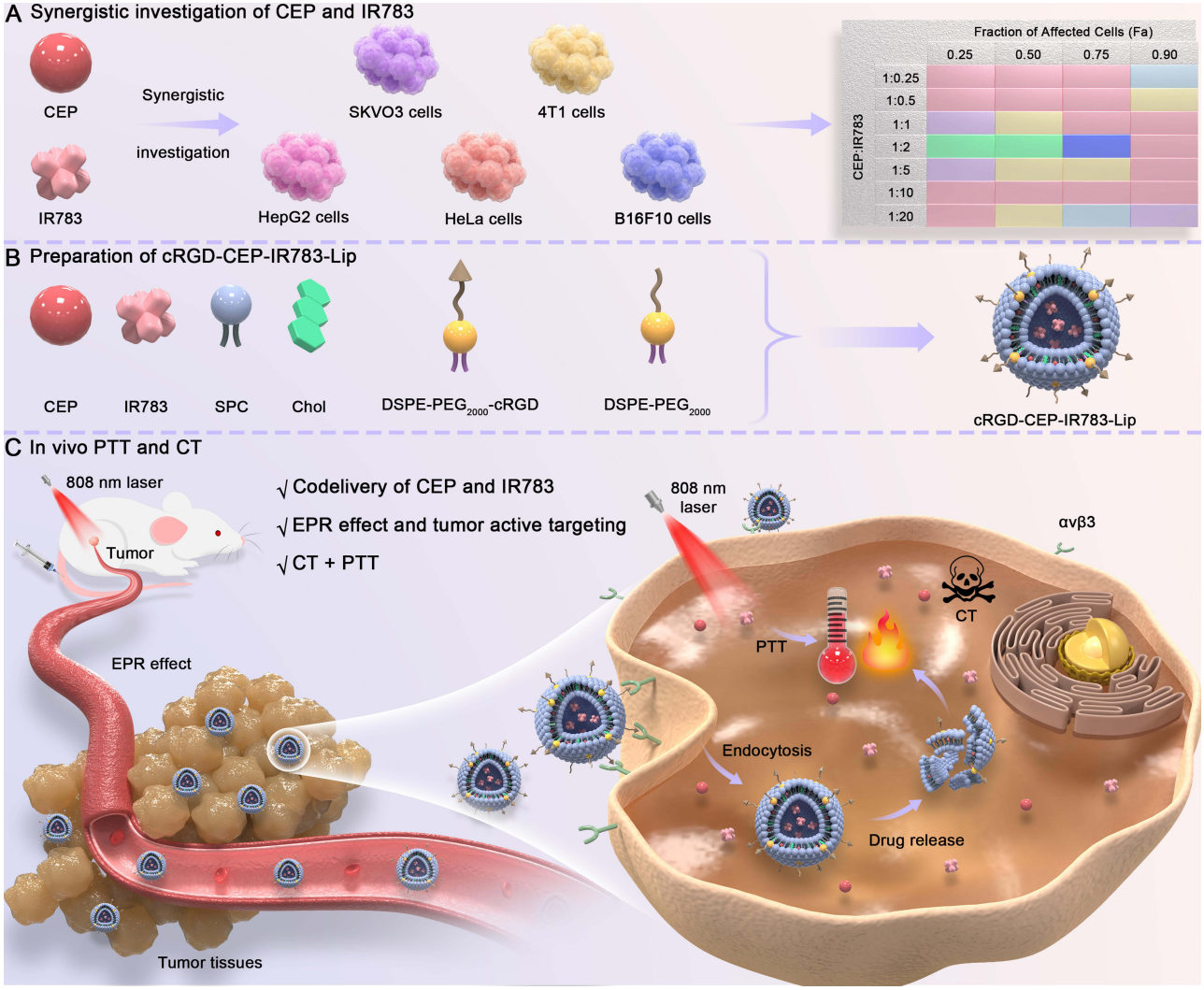


**Scheme 1** Schematic illustration of liposomes (Lip) loaded with cepharanthine (CEP) and IR783 for chemotherapy (CT) combined with photothermal therapy (PTT) for breast cancer. (**A**) Synergistic investigation of CEP and IR783. (**B**) Preparation of cRGD-CEP-IR783-Lip. SPC, soybean phosphatidylcholine; Chol, cholesterol. (**C**) The antitumor mechanism of cRGD-CEP-IR783-Lip after 808 nm laser irradiation via CT combined with PTT. EPR, enhanced permeability and retention.

tumor cell surface. The cRGD-CEP-IR783-Lip were obtained through the simultaneous loading of CEP and IR783 and were finally evaluated in vivo and in vitro for their combined therapeutic efficacy.

# Materials and Methods

## Materials

IR783 and CEP were purchased from Anhui Zesheng Technology Co., Ltd. (Anhui, China). Fetal bovine serum (FBS) and Dulbecco's modified Eagle's medium (DMEM) were purchased from Gibco (USA). Soybean phosphatidylcholine (SPC), DSPE-$PEG_{2000}$-cRGD, and DSPE-$PEG_{2000}$ were obtained from Shanghai Advanced Vehicle Technology Co., Ltd. (Shanghai, China). Trypsin-EDTA, phosphate buffered saline (PBS) and eosin staining solution were purchased from Beijing Solarbio Science and Technology Co., Ltd. (Beijing, China). Dimethyl sulfoxide (DMSO), hematoxylin, and 3-(4,5-dimethylthiazol-2-yl)-2,5-diphenyltetrazolium bromide (MTT) were purchased from Biosharp. Cholesterol (Chol) was purchased from Shanghai Adamas Reagent Co., Ltd. (Shanghai, China). Hoechst 33,342 was purchased from Shanghai Beyotime Biotechnology Co., Ltd. (Shanghai, China).

## Cells and Animals

The SKOV3 human ovarian adenocarcinoma, 4T1 mouse breast cancer, HepG2 human hepatocellular carcinoma, HeLa human cervical carcinoma, and B16F10 mouse melanoma cell lines were purchased from the American Type Culture Collection (Manassas, VA, USA). All cell lines were maintained in DMEM supplemented with 10% FBS and incubated at 37°C in a 5% $CO_2$ atmosphere with 90% relative humidity.

Healthy female BALB/c mice, 6–8 weeks old, were purchased from SPF (Beijing) Biotechnology Co., Ltd. (certificate number: SCXJ (Jing) 2019–0010, Beijing, China) and housed under a temperature of 23 ± 1°C with a relative humidity of 55 ± 5%. The animals were used for the experiments after a week of adaptation. The animal experiments were approved by the Animal Ethics Committee of Zunyi Medical University (approval number: Zunyi Lunshen (2020) 2–107). All experimental procedures and animal care were performed in accordance with the National Institutes of Health Guide for the Care and Use of Laboratory Animals.

## Determining the Optimal Synergistic Ratio for the CEP and IR783 Combination

The cytotoxicity of CEP and IR783, administered separately or in combination, was assessed in five cancer cell lines using the MTT assay. Cells were seeded in 96-well plates at a density of $3\times10^3$ to $5\times10^3$ cells/well and incubated for 24 h at 37°C in a 5% $CO_2$ incubator. IR783 and CEP were dissolved in DMSO to obtain a 10 mM stock solution. Subsequently, the culture medium was replaced with a medium containing the free drug (CEP or IR783) or one of seven different CEP:IR783 combinations (1:0.25, 1:0.5, 1:1, 1:2, 1:5, 1:10, and 1:20), and the cells were incubated for another 24 h. Thereafter, an 808 nm laser (MX-GX-808/5000 mW, Changchun Feimiao Technology Co., Ltd.) was used to irradiate each well for 1 min (0.4 $W/cm^2$). After irradiation was completed, the drug-containing medium was aspirated, and 10% MTT solution (5 mg/mL) was added to each well for 4 h. The MTT-containing medium was then aspirated, and 100 μL of DMSO was added to each well to determine the absorbance at a wavelength of 490 nm. The effects of CEP on the viability of the five cell types were examined using the same method, except that no laser was used. Cell viability was calculated as follows:

$$Cell\ viability\,(\%) = (A_s - A_b)/(A_s - A_b)\times 100$$

where $A_s$, $A_c$, and $A_b$ refer to the absorbance of the sample, control, and blank (PBS buffer), respectively.

The combination of CEP and IR783 was evaluated using the combination index (CI) method established by Chou and Talalay.[26–28] The CEP and IR783 combination effects were explained as follows: CI < 0.9, synergism; = 0.9–1.1, additive effect; > 1.1, antagonism (Supplementary Material).

## Preparation of Different Liposomes

cRGD-CEP-IR783-Lip were prepared using the thin-film dispersion-ultrasonic method. Briefly, a lipid mixture of SPC, Chol, DSPE-$PEG_{2000}$, and DSPE-$PEG_{2000}$-cRGD at a molar ratio of 61:31:2:6 was dissolved in 1 mL of a mixed organic solvent (chloroform/methanol = 2:1, v/v) in a 50 mL flask. CEP was added to the flask at a drug-to-lipid ratio of 1:30 and

then evaporated under reduced pressure to form a lipid film, which was then placed in a vacuum dryer overnight to completely remove the organic solvent. Subsequently, 1 mL of IR783 solution (in PBS buffer, 10 mM, pH 7.4) was added to the flask at a drug-to-lipid ratio of 1:10. The solution was placed in a constant-temperature shaker for approximately 40 min, and the suspension was ultrasonicated (195 W, 5 min). Finally, cRGD-CEP-IR783-Lip were obtained. PEG-CEP-IR783-Lip, PEG-IR783-Lip, and PEG-CEP-Lip were prepared using SPC, Chol, and DSPE-$PEG_{2000}$ at a molar ratio of 62:32:6. The preparation was performed as described above.

## Characterization of Liposomes

### Determination of Particle Size, Zeta Potential, and Morphology

The particle size, polydispersity index (PDI), and zeta potential of the prepared liposomes were determined using Brookhaven zeta potential and particle size analyzer (90 Plus PALS, Brookhaven, USA). Analyses were performed at (25 ± 0.2) °C, and all determinations were performed in triplicate. Subsequently, the morphology was studied using transmission electron microscopy (TEM) (JEM-1400 Plus, JEOL Ltd.).

### Determination of Encapsulation Efficiency and Drug Loading Content

The encapsulation efficiency (EE%) of the different formulations was measured using ultrafiltration centrifugation, and the drug loading content (DL%) was calculated using high-performance liquid chromatography (HPLC) (Supplementary Material). The determination method for the mobile phase composition of IR783 is shown in Table S1.

### In vitro Release Study

The in vitro release behavior of PEG-CEP-IR783-Lip and cRGD-CEP-IR783-Lip was studied using the dialysis method, and the concentrations of CEP and IR783 were determined according to validated HPLC methods (Supplementary Material).

### Stability of Liposomes

The prepared liposomes were maintained at 4°C for 7 d to determine the particle size and PDI. The changes in particle size and PDI of PEG-Blank-Lip and cRGD-Blank-Lip in PBS, 10% FBS, and DMEM were measured continuously over a 48 h period to investigate their stability in vivo.

### In vitro Photothermal Performance

To evaluate the influence of different laser powers on the photothermal effect of IR783 (0.5 mM), the IR783 solution was irradiated using an 808-nm laser under different power densities (0.00, 0.05, 0.10, 0.20, and 0.40 $W/cm^2$), and temperature changes in the solution were recorded. Thereafter, the temperature changes for different concentrations of IR783 (0.000, 0.100, 0.125, 0.250, and 0.500 mM) were investigated using an 808-nm laser (0.2 $W/cm^2$) within 500 s. In addition, three rounds of on/off laser irradiation (0.2 $W/cm^2$) were performed to evaluate the photostability of the IR783 solution (0.5 mM). The temperature of the solution during laser irradiation was monitored using a FOTRIC 220 infrared thermal imager.

### Cytotoxicity Assay

The 4T1 cells were seeded in 96-well plates at a density of $5\times10^3$ cells/well. After 24 h of culture, different concentrations of cRGD-CEP-IR783-Lip or PEG-CEP-IR783-Lip were added, and the cells were incubated for another 24 h. For laser irradiation groups, the cells were irradiated with a laser (808 nm, 0.4 $W/cm^2$) for 1 min per well. The culture medium was then discarded, and the cells were washed three times with PBS and incubated in a medium containing 10% MTT for 4 h. Finally, 100 μL of DMSO was added, and the absorbance at 490 nm was detected using a microplate reader.

### In vitro Cellular Uptake Study

To evaluate the cellular uptake of liposomes, 4T1 cells were seeded at a density of $3\times10^4$ cells/well in a cell culture dish. After the cells were cultured for 24 h, they were treated with PEG-IR783-Lip, cRGD-IR783-Lip, or free IR783 (concentration: 5 μM) and further incubated for 1, 2, 3, 4, 5, and 6 h. Next, the cells were washed three times with PBS, and 1 mL of DMEM was added to each well. Cellular uptake was analyzed using an LSM 900 confocal laser scanning microscope (Zeiss, Germany).

### Establishment of Tumor Model

A 4T1 tumor-bearing mouse model was established by subcutaneously injecting a 4T1 cell suspension ($1.0 \times 10^6$ cells) into the right dorsal region of each mouse. Subsequent experiments were initiated when the tumor volume reached 80–100 $mm^3$.

### In vivo Fluorescence and Photothermal Imaging

For in vivo fluorescence imaging, the prepared PEG-IR783-Lip and cRGD-IR783-Lip were intravenously injected (volume: 100 μL) into 4T1 tumor-bearing mice (IR783 dosage: 1 mg/kg). At 0, 2, 4, 8, 12, 24, and 48 h after administration, fluorescence imaging was performed using a NightOWL II LB983 small animal in vivo imaging system (Berthold Technologies GmbH & Co. KG). The imaging conditions were: $\lambda_{ex}$, 720 ± 20 nm; $\lambda_{em}$, 840 ± 20 nm; and exposure time, 0.1 s.

For photothermal imaging, the prepared PEG-IR783-Lip and cRGD-IR783-Lip were intravenously injected (volume: 100 μL) into 4T1 tumor-bearing mice (IR783 dosage: 5 mg/kg). An 808 nm laser (0.4 $W/cm^2$) was used to irradiate the tumor 8 h post-administration (550 s per mouse), and an infrared imager was used to record the thermal images and real-time temperature of the tumor.

### In vivo Anti-Tumor Therapy

Liposomes loaded with CEP and IR783 were prepared at a molar ratio of 1:2, and the CEP dosage was calculated to be 1 mg/kg. The 4T1 tumor-bearing mice were randomly divided into eight groups: PBS+laser, PBS, cRGD-CEP-IR783-Lip+laser, cRGD-CEP-IR783-Lip, PEG-CEP-IR783-Lip+laser, IR783+laser, CEP, and CEP-IR783+laser. For the "+laser" groups, the animals were intravenously injected with PBS, cRGD-CEP-IR783-Lip, PEG-CEP-IR783-Lip, IR783, and CEP-IR783. Furthermore, the tumor was irradiated with an 808 nm laser (0.4 $W/cm^2$, 8 min) at 8 h post-injection. The first laser irradiation was recorded as 0 d, and the tumor was irradiated at 0, 2, and 4 d. For the PBS, cRGD-CEP-IR783-Lip, and CEP groups, the animals were intravenously injected with PBS, cRGD-CEP-IR783-Lip, and CEP (100 μL/mouse), respectively. The experimental period was 14 d, and changes in the weight and tumor volume of the mice were recorded daily. After the weight and tumor size of the mice were recorded on the 14th day, blood was collected, the mice were sacrificed, and the liver and kidney function markers of the cRGD-CEP-IR783-Lip and PBS groups were measured. The major organs (heart, liver, spleen, lungs, and kidneys) and tumor tissues were stained with hematoxylin and eosin (H&E).

## Statistical Analysis

All data were expressed as the mean ± standard deviation. Statistical analyses were performed using ANOVA and the Student's *t*-test. A *p*-value <0.01, <0.001, and <0.0001 indicated statistical significance.

# Results and Discussion

## Defining the Synergistic Ratio of the CEP and IR783 Combination

### Evaluation of Cytotoxicity

To demonstrate the generalizability of our work, we used five types of cancer cell lines: human HepG2, SKVO3, and HeLa cells, and murine 4T1 and B16F10 cells. The effects of CEP and IR783 on cell viability were assessed in various cell lines using an MTT assay. The phototoxicity of IR783 was determined by 808 nm laser irradiation after incubation with different drug concentrations for 24 h. The $IC_{50}$ values were obtained from the dose-response curves for CEP and IR783 after 24 h of treatment (Figures S1 and S2). The respective $IC_{50}$ values for CEP and IR783 were as follows: SKVO3, 25.06 ± 1.81 μM and 19.21 ± 0.81 μM; HeLa, 38.33 ± 2.73 μM and 27.87 ± 3.21 μM; HepG2, 28.50 ± 0.81 μM and 14.52 ± 1.76 μM; 4T1, 33.99 ± 0.25 μM and 20.71 ± 1.90 μM; and B16F10, 10.32 ± 0.48 μM and 4.98 ± 1.98 μM. Notably, the results revealed a heightened sensitivity of B16F10 cells to the combination of free CEP and IR783 compared to other cell lines. The above data provide basic information for the subsequent calculation of CI values.

### Calculation of CI

The co-administration of drugs can elicit a spectrum of outcomes encompassing synergistic, additive, and antagonistic effects. Specifically, a synergistic effect refers to the combined action of drugs resulting in an effect greater than the sum of their individual effects, encapsulating the concept of "1 + 1 > 2". This synergy enables a reduction in drug dosage to a certain extent,

thereby mitigating the potential toxic side effects arising from elevated doses. The goal is to achieve maximal therapeutic efficacy using lower drug concentrations. The elucidation of data processing outcomes was guided by the approach outlined in a previous study.[29] The CI values are refined and presented in a heatmap format (Figure 1B). This representation aids in comprehending the results of the combined treatment with CEP and IR783 in a more visually intuitive manner.

The synergistic effects of CEP and IR783 were investigated in five cell lines (Figure 1A). A heatmap representation of the CI values for CEP and IR783 combination ratios in different cell lines and different fractions of affected cells (Fa) is shown in

A

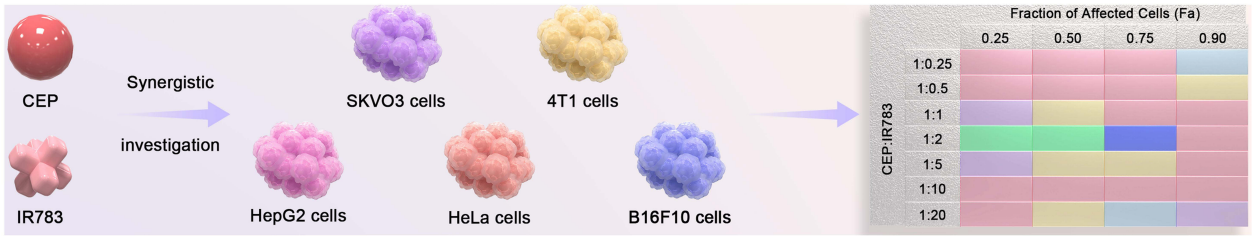


B

| Combination Index (CI) | >1.3 | 1.1-1.3 | 0.9-1.1 | 0.8-0.9 |
|---|---|---|---|---|
| Description of combination effect | Antagonism | Moderate antagonism | Additive | Slight synergism |
| Combination Index (CI) | 0.6-0.8 | 0.4-0.6 | <0.4 | |
| Description of combination effect | Moderate synergism | Synergism | Strong synergism | |

C

| Fraction of Affected Cells (Fa) (SKVO3) | | | | |
|---|---|---|---|---|
| CEP:IR783 | 0.25 | 0.50 | 0.75 | 0.90 |
| 1:0.25 | 0.10674 | 0.16323 | 0.28687 | 0.54709 |
| 1:0.5 | 0.22287 | 0.29979 | 0.50714 | 0.99836 |
| 1:1 | 0.25706 | 0.30830 | 0.46988 | 0.88338 |
| 1:2 | 0.07648 | 0.10318 | 0.16167 | 0.30418 |
| 1:5 | 0.21698 | 0.38196 | 0.72769 | 1.58847 |
| 1:10 | 0.02865 | 0.05525 | 0.11147 | 0.24601 |
| 1:20 | 0.34623 | 0.38642 | 0.44133 | 0.52944 |

D

| Fraction of Affected Cells (Fa) (4T1) | | | | |
|---|---|---|---|---|
| CEP:IR783 | 0.25 | 0.50 | 0.75 | 0.90 |
| 1:0.25 | 2.49933 | 1.92675 | 1.49882 | 1.17613 |
| 1:0.5 | 2.79007 | 2.06124 | 1.53637 | 1.15567 |
| 1:1 | 0.89665 | 1.30776 | 1.92069 | 2.84240 |
| 1:2 | 0.02982 | 0.16215 | 0.88564 | 4.86251 |
| 1:5 | 0.88868 | 1.05059 | 1.24471 | 1.47851 |
| 1:10 | 2.73733 | 2.58832 | 2.45029 | 2.32285 |
| 1:20 | 1.53173 | 1.26248 | 1.04119 | 0.85930 |

E

| Fraction of Affected Cells (Fa) (HepG2) | | | | |
|---|---|---|---|---|
| CEP:IR783 | 0.25 | 0.50 | 0.75 | 0.90 |
| 1:0.25 | 0.79457 | 0.43361 | 0.26143 | 0.17576 |
| 1:0.5 | 0.92875 | 0.44128 | 0.23378 | 0.13630 |
| 1:1 | 0.73545 | 0.57997 | 0.50293 | 0.46732 |
| 1:2 | 0.29144 | 0.28793 | 0.30447 | 0.33604 |
| 1:5 | 0.15410 | 0.20862 | 0.29251 | 0.41832 |
| 1:10 | 0.20993 | 0.31006 | 0.46686 | 0.71031 |
| 1:20 | 0.00521 | 0.02232 | 0.09672 | 0.42124 |

F

| Fraction of Affected Cells (Fa) (HeLa) | | | | |
|---|---|---|---|---|
| CEP:IR783 | 0.25 | 0.50 | 0.75 | 0.90 |
| 1:0.25 | 1.09536 | 0.54736 | 0.28104 | 0.14921 |
| 1:0.5 | 0.08567 | 0.12374 | 0.18176 | 0.27313 |
| 1:1 | 2.91643 | 1.54428 | 0.85604 | 0.51932 |
| 1:2 | 0.23983 | 0.31503 | 0.41592 | 0.55321 |
| 1:5 | 0.33148 | 0.53958 | 0.88016 | 1.44025 |
| 1:10 | 1.05462 | 0.92182 | 0.80641 | 0.70630 |
| 1:20 | 1.20853 | 1.16697 | 1.12731 | 1.08965 |

G

| Fraction of Affected Cells (Fa) (B16F10) | | | | |
|---|---|---|---|---|
| CEP:IR783 | 0.25 | 0.50 | 0.75 | 0.90 |
| 1:0.25 | 0.12674 | 0.16871 | 0.22529 | 0.30191 |
| 1:0.5 | 0.10498 | 0.14758 | 0.20855 | 0.29643 |
| 1:1 | 0.09833 | 0.14799 | 0.22441 | 0.34310 |
| 1:2 | 0.05968 | 0.12732 | 0.27410 | 0.59554 |
| 1:5 | 0.11247 | 0.21373 | 0.40950 | 0.79059 |
| 1:10 | 0.05052 | 0.11308 | 0.25458 | 0.57615 |
| 1:20 | 0.08809 | 0.21180 | 0.51111 | 1.23725 |

**Figure 1** Determining the optimal synergistic ratio for combining CEP and IR783. (**A**) Schematic of synergistic investigation for CEP and IR783 in five cell lines. (**B**) Schematic visualization of CI values: CI >1.3, antagonism, red; 1.1–1.3, moderate antagonism, pink; 0.9–1.1, light pink; 0.8–0.9, slight synergism, pale green; 0.6–0.8, moderate synergism, light green; 0.4–0.6, synergism, medium green; < 0.4, strong synergism, dark green. Heatmap of CI values for the fraction of affected cells (Fa) under different CEP and IR783 ratios in SKVO3 (**C**), 4T1 (**D**), HepG2 (**E**), HeLa (**F**), and B16F10 cells (**G**). CI values were calculated at different Fa values (ranging from 0 to 1), where Fa = 0 represents 100% viability, and Fa = 1 represents 0% viability.

Figure 1. CEP and IR783 showed synergistic effects on SKVO3 (Figure 1C), HepG2 (Figure 1E), and B16F10 cells (Figure 1G) at almost all ratios, whereas most ratios showed antagonistic effects on 4T1 cells (Figure 1D). Except for the 1:20 ratio, the combination ratios showed varying degrees of synergy with HeLa cells (Figure 1F). For anticancer agents, a higher effect level of Fa >0.8 was more relevant to treatment because complete eradication of cancer cells was the ideal treatment outcome.[29–32] For all cells, we could easily obtain an optimal ratio of their Fa values above 0.75. For example, for SKVO3 cells at an Fa of 0.9, five ratios played synergistic roles, among which 1:2 and 1:10 were strongly synergistic (Figure 1C). For SKVO3 cells, an Fa of 0.75 was taken as an example; although different ratios showed various degrees of synergistic effects, 1:0.25, 1:2, and 1:10 showed strong synergistic effects. However, when the Fa was 0.9, the effect changed from synergistic to antagonistic at a ratio of 1:5. These findings showed that different ratios and Fa values could indicate a variety of situations, including reversals (Figure 1C). In 4T1 cells, only 1:2 showed a slight synergistic effect when the Fa was 0.75, whereas only 1:20 showed a slight synergistic effect when the Fa was 0.9. However, when the Fa was 0.5, the 1:2 ratio showed a strong synergistic effect (Figure 1D). For anticancer or antiviral agents, synergy at high effect levels (eg, Fa > 0.8) is more relevant to therapy than at low effect levels (eg, Fa < 0.2).[28] In general, the combination of CEP and IR783 at a ratio of 1:2 showed a synergistic effect in all five cell types at an Fa of 0.75, indicating that it was feasible to achieve synergistic therapy at the cellular level. Therefore, the drug ratio in the subsequent experiments was set at 1:2.

## Characterization of Liposomes

### Determination of Particle Size, Zeta Potential and Morphology

Liposomes were prepared using the thin-film dispersion-ultrasonic method (Figure 2A), and the particle size, PDI, and zeta potential of the liposomes were determined using dynamic light scattering. As shown in Table S2, the average particle size of cRGD-CEP-IR783-Lip was 120.05 ± 1.48 nm, and the zeta potential was –38.03 ± 0.38 mV, thus demonstrating good stability. The particle size of cRGD-modified liposomes was slightly greater than that of unmodified liposomes. Moreover, the zeta potential did not change significantly. All liposomes were negatively charged, which could reduce nonspecific cellular uptake and prolong circulation time due to electrostatic repulsion with negatively charged cell membrane surfaces.[33] In addition, TEM results showed that the liposomes had a near-spherical shape consistent with the particle size determination and a normal particle size distribution (Figure 2B and C), indicating that they could be targeted to tumor through EPR effects.[34]

### Determination of Encapsulation Efficiency and Drug Loading Content

The EE% was measured using the ultrafiltration centrifugation method. The results showed that CEP and IR783 were encapsulated in liposomes with an EE% greater than 85%. The EE% of cRGD-modified liposomes did not decrease compared with that of unmodified liposomes, indicating that cRGD surface modification had no effect (Table S3). To achieve optimal synergy between the two drugs, we maintained a molar ratio of 1:2 for CEP:IR783, resulting in a drug loading ratio of 3.30 ± 0.14% (w/v) for CEP and 8.68 ± 0.12% (w/v) for IR783 (Table S3). The cRGD modification did not change the drug loading capacity, which led to a drug loading ratio of 2.91 ± 0.00% (w/v) for CEP and 7.40 ± 0.13% (w/v) for IR783 (Table S3). These results are consistent with those reported in the literature.[35]

### In vitro Release Study

The concentrations of CEP and IR783 in the release medium were determined using HPLC. As shown in Figure 2D and E, the release behaviors of cRGD-CEP-IR783-Lip and PEG-CEP-IR783-Lip at 12 h were similar, with cumulative release rates of 40% for CEP and 10% for IR783. At 36 h, the drugs released from PEG-CEP-IR783-Lip and cRGD-CEP-IR783-Lip tended to be stable, with cumulative release rates of approximately 50% for CEP and 30% for IR783. Compared to PEG-CEP-IR783-Lip, cRGD-CEP-IR783-Lip did not cause a sudden release of CEP and IR783, although the peptide cRGD was modified on the surface of the liposomes. The above experiments showed that cRGD did not change the drug release behavior of liposomes and could steadily and continuously release drugs into the release medium. In general, traditional unmodified liposomes do not have the ability for pH-controlled release.[33,36,37] Therefore, our liposomes were only modified with cRGD to confer tumor-targeting ability relative to conventional liposomes. In addition, the difference in pH between tumor tissues (~6.5) and normal tissues (~7.4) was small; therefore, it was presumed that drug release from cRGD-modified liposomes was less affected by pH.

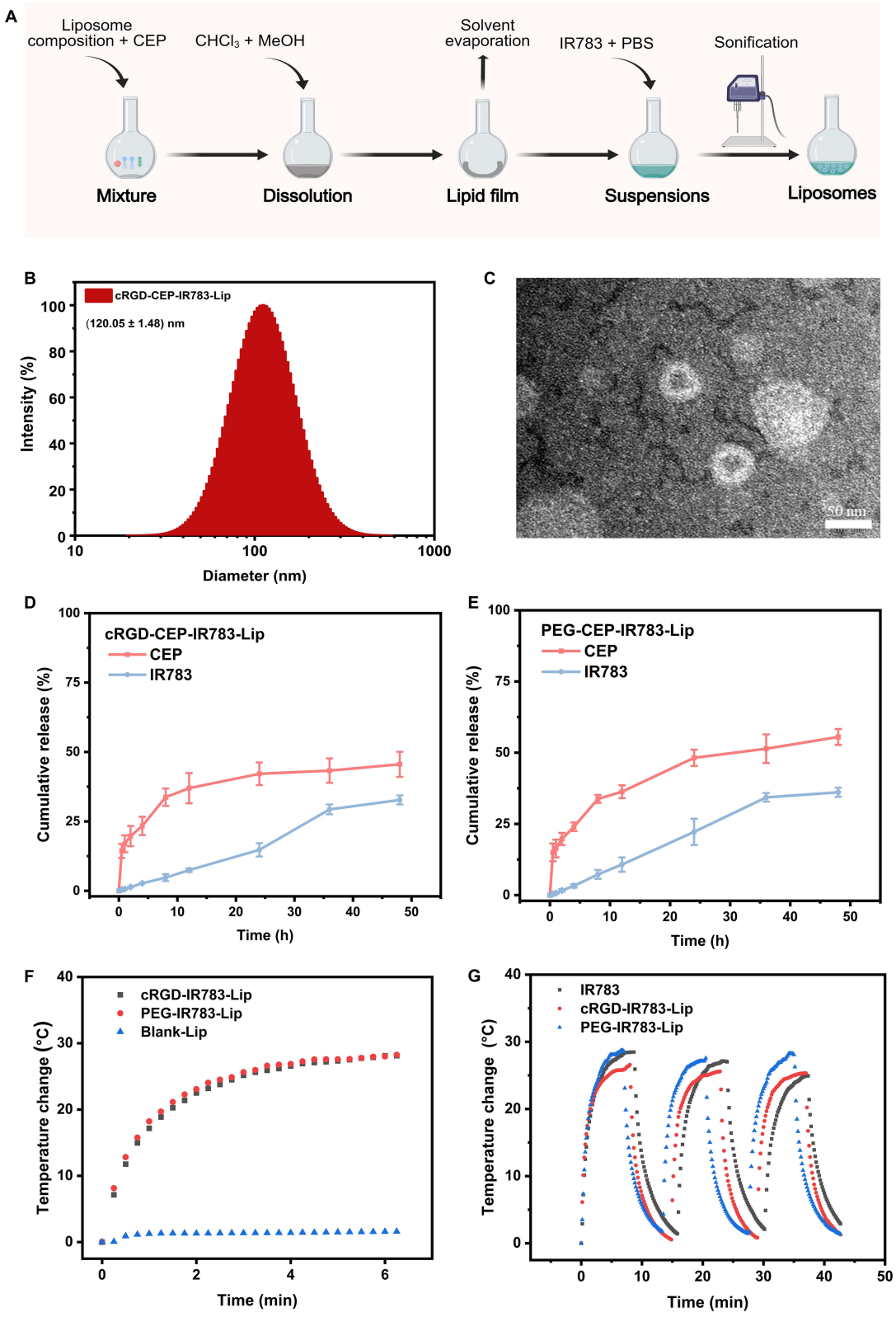


**Figure 2** Characterization, in vitro release, and photothermal properties of cRGD-CEP-IR783-Lip. (**A**) Schematic diagram of the preparation of cRGD-CEP-IR783-Lip. (**B**) Size distribution of cRGD-CEP-IR783-Lip. (**C**) Morphology image of cRGD-Blank-Lip by TEM. (**D**) In vitro release of CEP and IR783 in cRGD-CEP-IR783-Lip (n = 3). (**E**) In vitro release of CEP and IR783 in PEG-CEP-IR783-Lip (n = 3). (**F**) Photothermal heating curves of cRGD-IR783-Lip, PEG-IR783-Lip, and Blank-Lip under 808 nm irradiation (0.2 W/cm$^2$) for 375 s. (**G**) Photothermal heating curves of IR783, PEG-IR783-Lip, and cRGD-IR783-Lip under three on/off cycles of 808 nm irradiation (0.2 W/cm$^2$).

### Stability of Liposomes

The changes in particle size and PDI of liposomes within 7 d at 4°C are shown in Figure S3. The results showed that the prepared liposomes had good stability. The particle size and PDI results for PEG-Blank-Lip and cRGD-Blank-Lip in 10% FBS and DMEM are shown in Figures S4 and S5. The liposomes showed good stability in 10% FBS and DMEM for 48 h, indicating no aggregation or disaggregation in the presence of serum. This finding is mainly attributed to the fact that DSPE-$PEG_{2000}$ improves the surface properties of liposomes and avoids recognition by macrophages of the mononuclear phagocytic system.[38] Therefore, the prepared liposomes showed no significant change in particle size and PDI during the experimental period in different media, thus providing an experimental basis for in vitro and in vivo experiments.

## In vitro Photothermal Performance

The investigation of the photothermal characteristics of IR783 involved analyzing solutions at varying power densities and concentrations. According to the data presented in Figure S6, there was a notable acceleration in the rate of temperature increase, which correlated with higher laser power densities and higher concentrations of IR783. To determine whether the photothermal properties of IR783 were affected by liposome loading, the photothermal conversion efficiency of Blank Lip, PEG-IR783-Lip, and cRGD-IR783-Lip and the photostability of free IR783, PEG-IR783-Lip, and cRGD-IR783-Lip were measured. The temperature of lipid materials at the same concentration did not increase significantly after laser irradiation (Figure 2F), and the photothermal properties of IR783 were not affected. When the 808 nm laser was turned on for 8 min, the temperatures of IR783, PEG-IR783-Lip, and cRGD-IR783-Lip increased quickly. In contrast, once the 808 nm laser was switched off, the temperatures of PEG-IR783-Lip and cRGD-IR783-Lip decreased to room temperature within 5 min (Figure 2G), indicating that the temperatures of these liposomes could be well controlled by the laser. However, in the free IR783 group, the time required to decrease the temperature to room temperature was 8 min. The temperature changes did not show any obvious differences between PEG-IR783-Lip and cRGD-IR783-Lip after three on/off cycles, indicating good photothermal stability and repeatability. However, temperature changes showed obvious differences in the free IR783 group. These results demonstrate that liposomes loaded with IR783 have excellent photothermal conversion ability and photostability.

## Cytotoxicity Assay

To evaluate the cytotoxicity of PEG-IR783-CEP-Lip and cRGD-IR783-CEP-Lip in 4T1 cells, an MTT assay was performed (Figure 3A). As shown in Figure 3B, PEG-CEP-IR783-Lip and cRGD-CEP-IR783-Lip, with or without laser irradiation, demonstrated dose-dependent cytotoxicity in 4T1 cells. The cytotoxicity of cRGD-CEP-IR783-Lip was higher than that of PEG-IR783-CEP-Lip at the same concentration under almost all concentrations tested. Moreover, cytotoxicity was stronger in the irradiated group than that in the non-irradiated group.

## In vitro Cellular Uptake Study

The uptake of free IR783, PEG-IR783-Lip, and cRGD-IR783-Lip by 4T1 cells was investigated using confocal laser scanning microscopy. Fluorescence imaging of free IR783 at different incubation times and statistics of the average fluorescence intensity (FI) are shown in Figure 3C, which indicates that the FI gradually increased with increasing incubation time. The results of PEG-IR783-Lip and cRGD-IR783-Lip are shown in Figure 3D and E, respectively. The uptake capacity of cells was similar to that of free IR783, and the intracellular FI gradually increased with increasing incubation time. The FI of cRGD-IR783-Lip was significantly higher than that of PEG-IR783-Lip and free IR783, indicating that cRGD-IR783-Lip had a better cellular uptake capacity. Loading IR783 with liposomes did not affect the uptake of IR783. Thus, the functionalization of cRGD on the surface of liposomes may promote their accumulation in cells.

## In vivo Fluorescence and Photothermal Imaging

In vivo fluorescence and photothermal imaging were performed on 4T1-bearing mice (Figure 4A). As shown in Figure 4B, obvious fluorescence was observed in the tumor 2 h after injection. The FI of cRGD-IR783-Lip was significantly higher than

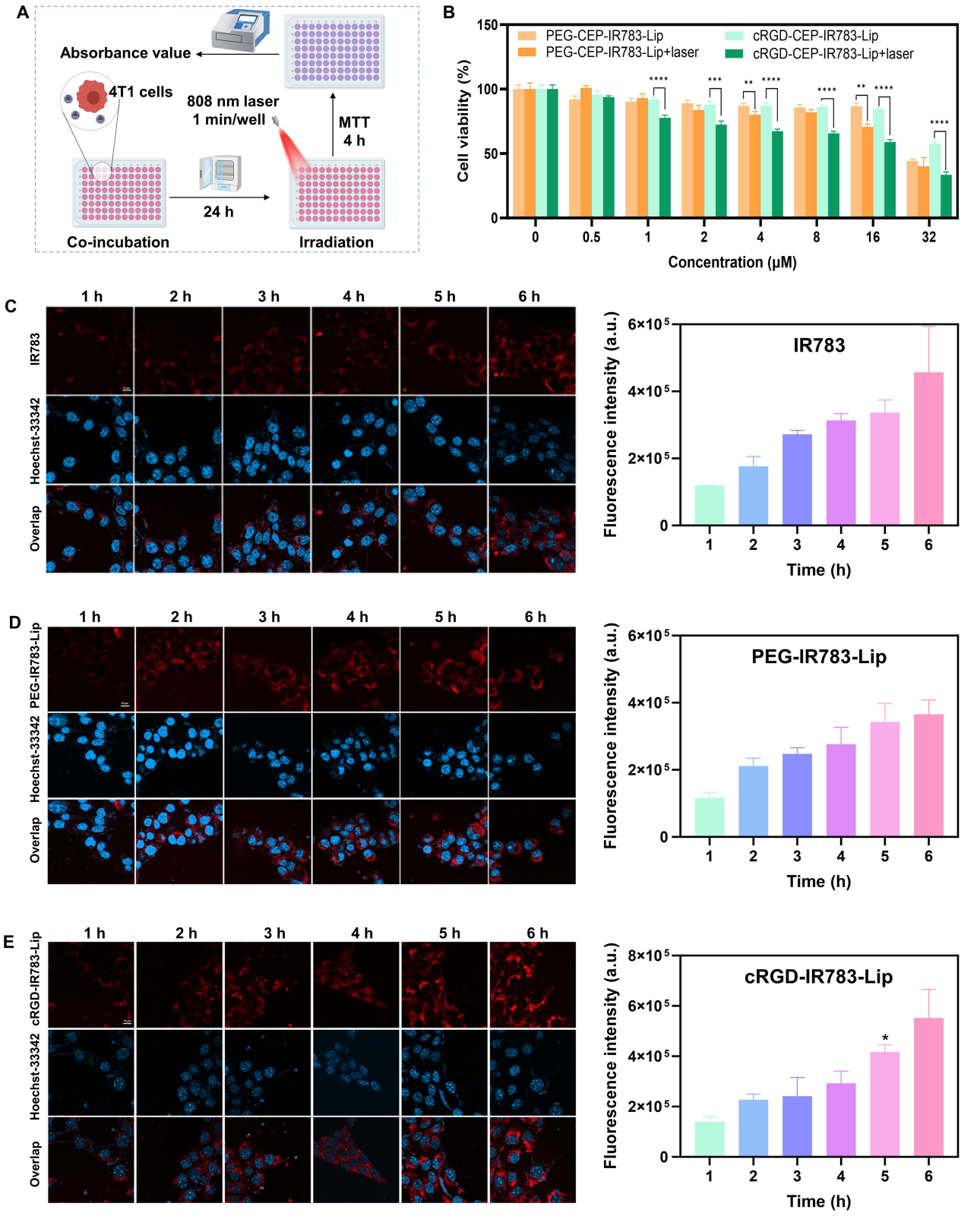


**Figure 3** Cytotoxicity and cellular uptake investigation. (**A**) Schematic diagram of the cytotoxicity assay. (**B**) Effect of cRGD-modified liposomes on the viability of 4T1 cells with and without laser irradiation (n = 5). Compared with the non-irradiated group, $^{**}p < 0.01$, $^{***}p < 0.001$, and $^{****}p < 0.0001$. confocal laser scanning microscopy images and fluorescence intensity analysis of free IR783 (**C**), PEG-IR783-Lip (**D**), and cRGD-IR783-Lip (**E**) incubated with 4T1 cells for different times (red); the nuclei were stained with Hoechst-33,342 (blue). Compared with the IR783 group, $^{*}p < 0.05$. Concentration of IR783: 5 μM; scale bar: 10 μm.

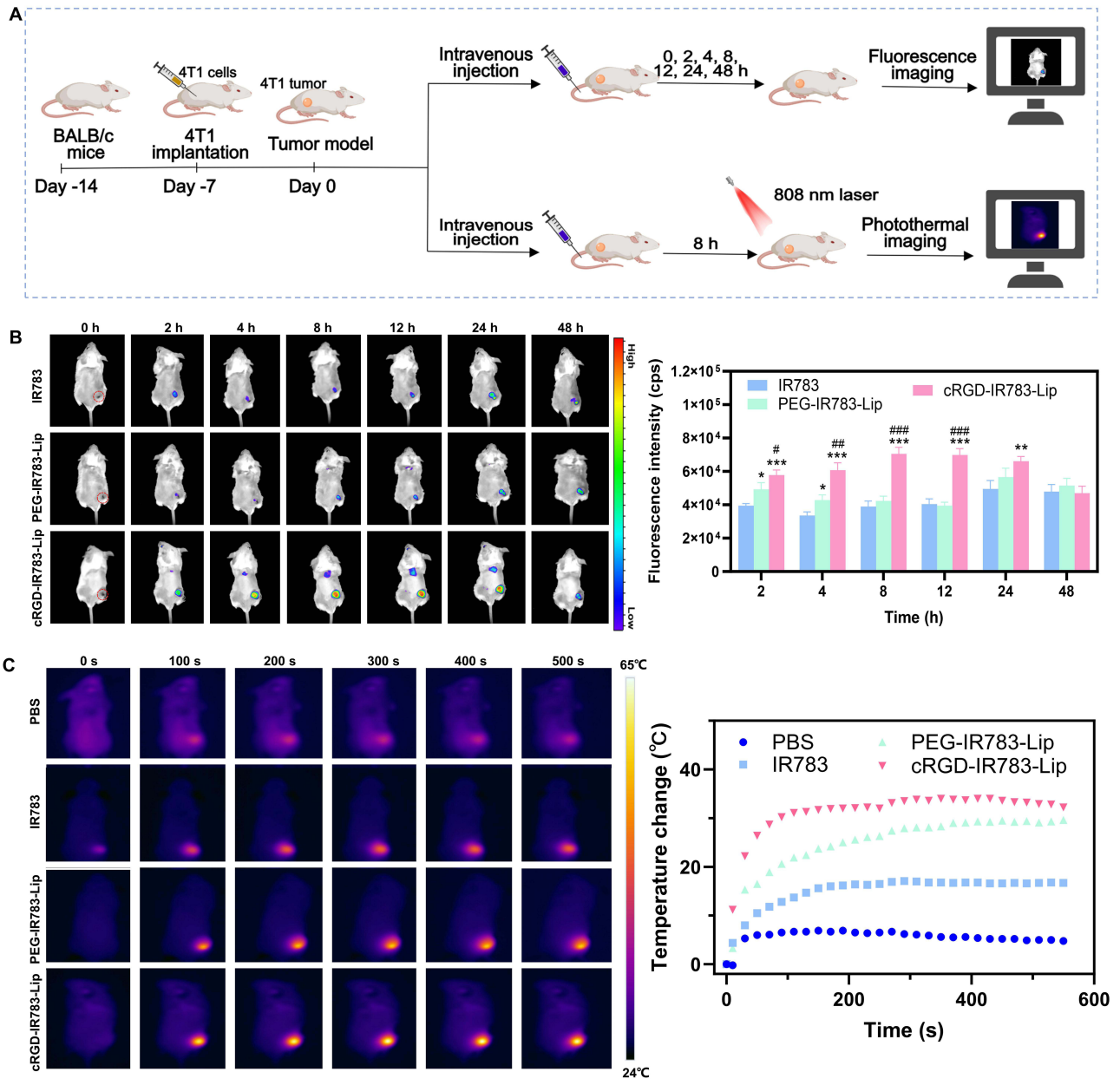


**Figure 4** Fluorescence and photothermal imaging in vivo. (**A**) Schematic diagram of fluorescence and photothermal imaging in vivo. (**B**) Fluorescence imaging and intensity of tumor-bearing mice at different time points after intravenous injection of free IR783, PEG-IR783-Lip, or cRGD-IR783-Lip (n = 5). Compared with the IR783 group, $^{*}p < 0.05$, $^{**}p < 0.01$, and $^{***}p < 0.001$; compared with the PEG-IR783-Lip group, $^{\#}p < 0.05$, $^{\#\#}p < 0.01$, and $^{\#\#\#}p < 0.001$. (**C**) Temperature curve of the tumor after laser irradiation.

that of free IR783 and PEG-IR783-Lip. Fluorescence at the tumor site did not decrease significantly at 24 h, but the fluorescence signal weakened at 48 h. In addition, cRGD-IR783-Lip exhibited good tumor targeting and long-term retention in vivo and could be used for tumor-targeted therapy. Mice were dissected 8 h after intravenous injection, and fluorescence imaging of the major organs and tumor tissues was performed. The results (Figure S7) corresponded to the in vivo fluorescence imaging results, showing strong fluorescence signals in the tumor tissues.

In vivo fluorescence imaging experiments confirmed the excellent tumor-targeting performance of cRGD-IR783-Lip. The distribution of PEG-IR783-Lip and cRGD-IR783-Lip in the in vivo fluorescence imaging was essentially the same, mainly due to their in vivo circulation time and particle size. Both liposomes were modified with DSPE-$PEG_{2000}$ to prolong in vivo circulation, and the particle size remained similar, which explains the consistency of their distribution in vivo. Based on PEG-IR783-Lip, cRGD-IR783-Lip was modified with functionalized cRGD polypeptides to enhance

the uptake of liposomes by tumor cells; thus, the FI of cRGD-IR783-Lip at the tumor was higher than that of free IR783 and PEG-IR783-Lip. In vitro fluorescence imaging of the major organs showed a weak fluorescence signal in the liver; this result may be attributed to the accumulation of liposomes in the liver following circulation and metabolism in the liver and intestine. Therefore, it is necessary to further investigate functional toxicity in the liver and kidney.

cRGD-IR783-Lip showed good in vitro photothermal properties and could target tumors and accumulate effectively through the EPR effect and active tumor targeting. Therefore, the photothermal properties were investigated in vivo, and free IR783, PEG-IR783-Lip, and cRGD-IR783-Lip were injected intravenously into 4T1-bearing mice. At 8 h post-injection, an 808 nm laser was used to irradiate the tumor. Thermal imaging was conducted using an infrared camera to monitor the real-time temperature of the tumors in mice. The temperature of the mice before 808 nm irradiation was 30.5 ± 0.2°C. As shown in Figure 4C, the temperature of cRGD-IR783-Lip rapidly increased by 32°C within 200 s of irradiation, and there was no downward trend within 500 s. The temperature of PEG-IR783-Lip increased by 24°C within 200 s, whereas the temperatures of free IR783 and PBS solution only increased by 16°C and 5°C, respectively. These results further demonstrate the superiority of functionalized liposomes modified by cRGD for tumor targeting.

## In vivo Anti-Tumor Therapy

Based on the good tumor targeting and imaging ability of liposomes in vivo and in vitro, the antitumor effects were further evaluated (Figure 5A). Laser irradiation had no effect on tumor growth in the PBS and PBS+laser groups (Figure 5B). Without laser irradiation, IR783 had no significant inhibitory effect on tumors. Moreover, the tumor inhibition effect of CEP and cRGD-CEP-IR783-Lip without irradiation was very limited, because CEP has no obvious tumor inhibition effect.[39] CEP was used in combination with IR783 mainly so that it could reverse P-glycoprotein-mediated multidrug resistance and increase the sensitivity of anticancer drugs.[40] As can be seen from Figure 5B–D, the tumor volume and weight were the smallest in the cRGD-CEP-IR783-Lip+laser group, indicating the most significant tumor suppression effect. There was no significant change in the body weight of the mice in each group during the treatment period, indicating that the drugs and laser irradiation had no effect on mouse growth (Figure S8). The major organs were stained with H&E (Figure 5E). The liver and kidney function markers in each group were alanine aminotransferase (ALT), aspartate aminotransferase (AST), and AST/ALT (Figure S9A–C), and the renal function markers were uric acid, urea, and creatinine (Figure S9D–F). The results showed that there was no significant hepatorenal functional toxicity in the experimental groups compared to the control group. In addition, the hemolysis of liposomes was investigated, and hemolysis of less than 10% was regarded as non-toxic.[41] As shown in Figure S10, the hemolysis rate remained below 10%, indicating a favorable biosafety profile of the liposomes. Collectively, these experimental results confirmed the biosafety of the liposomes.

The results of the in vivo and in vitro studies showed that cRGD-CEP-IR783-Lip had good tumor-targeting properties and a good tumor growth inhibition effect. The synergistic mechanism of CEP as a chemotherapeutic agent and IR783 as a photothermal agent in antitumor treatment may stem from the mutually reinforcing effects of PTT and chemotherapy. Indeed, studies have shown that PTT enhances the efficacy of chemotherapy.[8,42,43] Anticancer drugs may exhibit synergistic effects with heat, increasing cytotoxicity at elevated temperatures. This synergy directly boosts the lethality of the drug through the heat generated by PTT. Additionally, PTT improves the absorption of nanocarriers by tumor cells and speeds up drug release, subsequently increasing the intracellular drug concentration and cytotoxicity.[44–46] CEP offers a broad spectrum of anticancer activities, such as inhibiting cell proliferation, promoting apoptosis, and suppressing angiogenesis, and can trigger autophagy-related cell death in various cancer cell types.[23,24] Furthermore, CEP can modulate drug transporter proteins, such as P-glycoprotein, thereby enhancing drug accumulation in tumor cells.

However, the combined action of CEP and IR783 in the complex in vivo physiological environment requires more rigorous investigation, and whether their interaction at the tumor level can achieve a synergistic effect, as anticipated by the proposed 1:2 ratio, remains unclear. Therefore, further verification is needed to evaluate the in vivo antitumor activity of cRGD-CEP-IR783-Lip at an optimal synergistic molar ratio. In this study, H&E staining and liver and kidney function markers were detected in the cRGD-CEP-IR783-Lip and PBS groups after antitumor treatment, and no obvious organ injury or liver and kidney function toxicity was observed. Preliminary safety was investigated; however, the long-term cumulative toxicity, acute toxicity, and kinetics require further investigation.

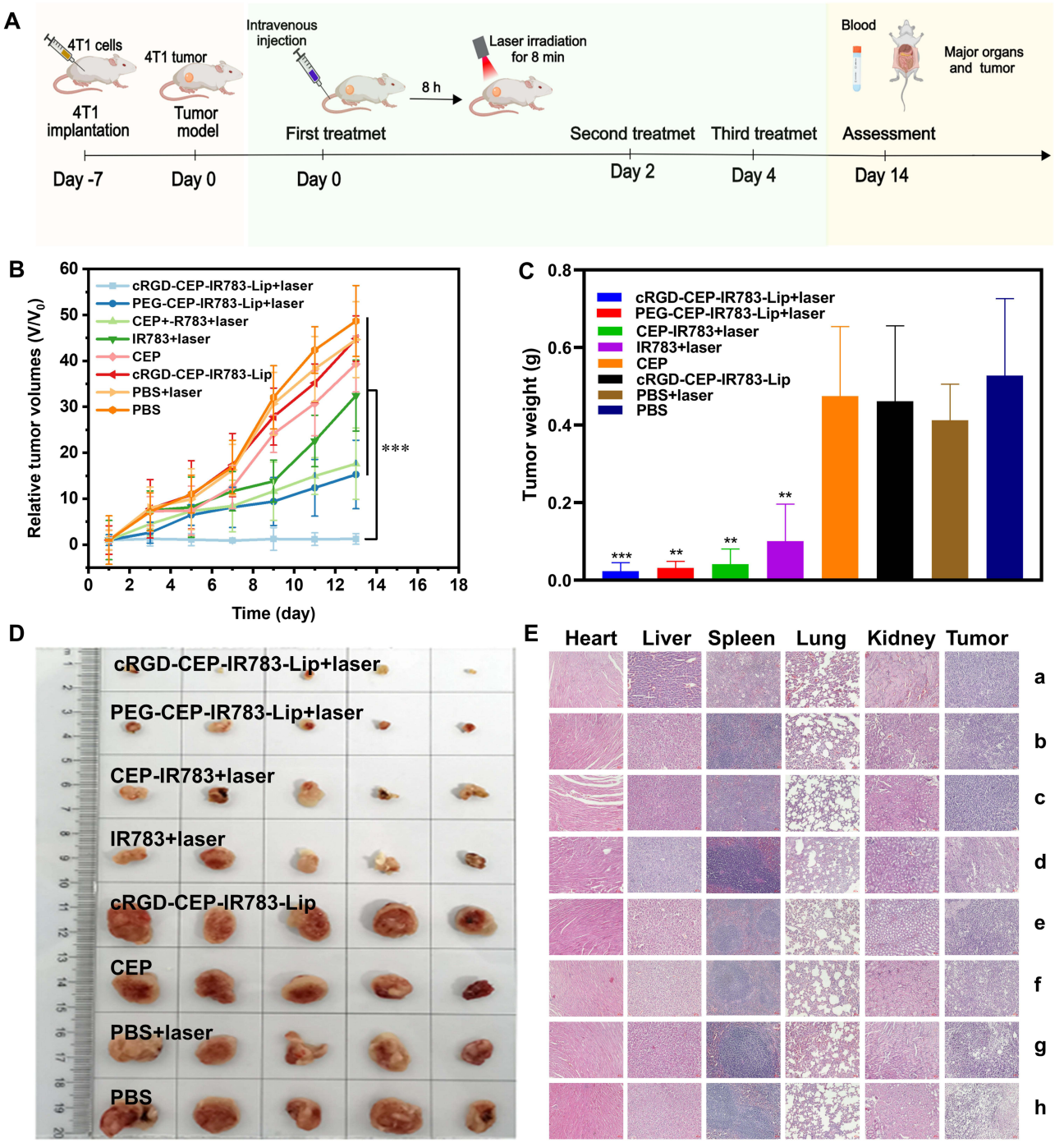


**Figure 5** In vivo therapeutic effect of cRGD-CEP-IR783-Lip on 4T1 tumor-bearing mice. (**A**) Schematic illustration of the antitumor study. (**B**) Changes in tumor volume across different treatment groups over a 14-d period. (**C**) Tumor weight after completion of treatment (n = 5). Compared with the PBS group, $^{**}p < 0.01$ and $^{***}p < 0.001$. (**D**) The tumor tissue was dissected and photographed after treatment. (**E**) The H&E staining images of the major organs and tumors in each group: (a) CEP, (b) IR783+laser, (c) PBS, (d) PBS+laser, (e) CEP-IR783+laser, (f) PEG-CEP-IR783-Lip+laser, (g) cRGD-CEP-IR783-Lip, and (h) cRGD-CEP-IR783-Lip+laser. Scale bar: 20 μm.

## Conclusion

In summary, we engineered multifaceted tumor-targeting dual-drug liposomes (cRGD-CEP-IR783-Lip), paving the way for the systematic exploration of the combined effects of CEP and IR783. Through comprehensive experimentation, the optimal synergistic molar ratio of CEP to IR783 was determined to be 1:2 across five distinct cell lines. This achievement underscores the capacity to achieve tumor selectivity and precise co-localized delivery of CEP and IR783 while maintaining a consistent synergistic ratio by utilizing cRGD-functionalized liposomes as a versatile platform. By strategically combining chemotherapy

and phototherapy, a discernible enhancement in the efficacy of in vivo antitumor therapy was achieved. This approach not only demonstrated the ability to inhibit tumor growth but also significantly reduced the required dosage of chemotherapy drugs, amplifying therapeutic benefits while concurrently mitigating potential adverse effects. Despite the potential of dual-drug-loaded liposomes, their clinical translation faces challenges, including inconsistent preparation and uncertainty about drug release at the tumor site. Nevertheless, our findings are expected to help overcome these obstacles.

## Acknowledgments

This work was supported by the Guizhou Province Science and Technology Plan Project (grant no. Qiankehe platform talents [2018] 5772-031), the Science and Technology Project of Traditional Chinese Medicine and Ethnic Medicine of Guizhou Province Administration of Traditional Chinese Medicine (grant no. QZYY-2021-079), the Guizhou Province College youth science and technology talents growth project (grant No. Qianjiaohe KY [2022] 274), the Science and Technology Foundation of Health Commission of Guizhou Province (grant no. gzwjkj2020-1-212), the Zunyi Science and Technology Plan Project (grant no. Zunshi Keren Platform [2023] 2), and the Science and Technology Innovation Team of Higher Education of Guizhou Provincial Education Department (grant no. Qianjiaoji [2023]073).

## Disclosure

The authors report no conflicts of interest in this work.

## References

1. Yu C, Kong L, Tian J, et al. Photoacoustic imaging-guided triple-responsive nanoparticles with tumor hypoxia relief for improving chemotherapy/photothermal/photodynamic synergistic therapy against breast cancer. *Biomed Pharm*. 2023;164:114928. doi:10.1016/j.biopha.2023.114928
2. Xia HY, Li BY, Ye YT, Wang SB, Chen AZ, Kankala RK. Transition metal oxide-decorated MXenes as drugless nanoarchitectonics for enriched nanocatalytic chemodynamic treatment. *Adv Healthcare Mater*. 2024;13:10. doi:10.1002/adhm.202303582
3. Kankala RK, Liu CG, Chen AZ, et al. Overcoming multidrug resistance through the synergistic effects of hierarchical pH-sensitive, ROS-generating nanoreactors. *ACS Biomater Sci Eng*. 2017;3(10):2431–2442. doi:10.1021/acsbiomaterials.7b00569
4. Pasha N, Turner NC. Understanding and overcoming tumor heterogeneity in metastatic breast cancer treatment. *Nat Cancer*. 2021;2(7):680–692. doi:10.1038/s43018-021-00229-1
5. Duan C, Yu M, Xu J, Li B-Y, Zhao Y, Kankala RK. Overcoming cancer multi-drug resistance (MDR): reasons, mechanisms, nanotherapeutic solutions, and challenges. *Biomed. Pharm*. 2023;162:114643. doi:10.1016/j.biopha.2023.114643
6. Yao J, Zheng F, Yao C, et al. Rational design of nanomedicine for photothermal-chemodynamic bimodal cancer therapy. *Wiley Interdiscip Rev Nanomed Nanobiotech*. 2021;13(3):e1682. doi:10.1002/wnan.1682
7. Feng Q, Xu J, Zhuang C, Xiong J, Wang H, Xiao K. Mitochondria-targeting and multiresponsive nanoplatform based on AIEgens for synergistic chemo-photodynamic therapy and enhanced immunotherapy. *Biomacromolecules*. 2023;24(2):977–990. doi:10.1021/acs.biomac.2c01416
8. Fan W, Yung B, Huang P, Chen X. Nanotechnology for multimodal synergistic cancer therapy. *Chem Rev*. 2017;117(22):13566–13638. doi:10.1021/acs.chemrev.7b00258
9. Gu W, Meng F, Haag R, Zhong Z. Actively targeted nanomedicines for precision cancer therapy: concept, construction, challenges and clinical translation. *J Control Release*. 2021;329:676–695. doi:10.1016/j.jconrel.2020.10.003
10. Liu C-G, Han Y-H, Kankala RK, Wang S-B, Chen A-Z. Subcellular performance of nanoparticles in cancer therapy. *Int j Nanomed*. 2020;15:675–704. doi:10.2147/IJN.S226186
11. Ma Z, Li N, Zhang B, et al. Dual drug-loaded nano-platform for targeted cancer therapy: toward clinical therapeutic efficacy of multifunctionality. *J Nanobiotech*. 2020;18(1):123. doi:10.1186/s12951-020-00681-8
12. Zhou W, Zhou Y, Chen X, et al. Pancreatic cancer-targeting exosomes for enhancing immunotherapy and reprogramming tumor microenvironment. *Biomaterials*. 2021;268:120546. doi:10.1016/j.biomaterials.2020.120546
13. Yunus Basha R, K TSS, Doble M. Dual delivery of tuberculosis drugs via cyclodextrin conjugated curdlan nanoparticles to infected macrophages. *Carbohydr Polym*. 2019;218:53–62. doi:10.1016/j.carbpol.2019.04.056
14. Torchilin V. Tumor delivery of macromolecular drugs based on the EPR effect. *Adv. Drug Delivery Rev*. 2011;63(3):131–135. doi:10.1016/j.addr.2010.03.011
15. Prabhakar U, Maeda H, K JR, et al. Challenges and key considerations of the enhanced permeability and retention effect for nanomedicine drug delivery in oncology. *Cancer Res*. 2013;73(8):2412–2417. doi:10.1158/0008-5472.CAN-12-4561
16. Maeda H. Toward a full understanding of the EPR effect in primary and metastatic tumors as well as issues related to its heterogeneity. *Adv. Drug Delivery Rev*. 2015;91:3–6. doi:10.1016/j.addr.2015.01.002
17. Perry JL, Reuter KG, Luft JC, Pecot CV, Zamboni W, DeSimone JM. Mediating passive tumor accumulation through particle size, tumor type, and location. *Nano Lett*. 2017;17(5):2879–2886. doi:10.1021/acs.nanolett.7b00021
18. Chen L, Hong W, Ren W, Xu T, Qian Z, He Z. Recent progress in targeted delivery vectors based on biomimetic nanoparticles. *Signal Transduct Target Ther*. 2021;6(1):225. doi:10.1038/s41392-021-00631-2
19. Fang RH, Gao W, Zhang L. Targeting drugs to tumours using cell membrane-coated nanoparticles. *Nat Rev Clin Oncol*. 2023;20(1):33–48. doi:10.1038/s41571-022-00699-x
20. Huang Y, Xu L, Zhang F, et al. Preparation and pharmacokinetics in vivo of linarin solid dispersion and liposome. *Chin Herb Med*. 2022;14(2):310–316. doi:10.1016/j.chmed.2021.12.004

21. Cisterna BA, Kamaly N, Choi WI, Tavakkoli A, Farokhzad OC, Vilos C. Targeted nanoparticles for colorectal cancer. *Nanomedi*. 2016;11(18):2443–2456. doi:10.2217/nnm-2016-0194
22. Donnette M, Venton G, Farnault L, et al. Pharmacokinetics/pharmacodynamics of liposomal cytarabine (VYXEOS) in AML patients: influence of cytidine deaminase genetic polymorphisms. *J Clin Oncol*. 2020;38(15_suppl):e19517–e19517. doi:10.1200/JCO.2020.38.15_suppl.e19517
23. Liu Y, Xie Y, Lin Y, et al. Cepharanthine as a potential novel tumor-regional therapy in treating cutaneous melanoma: Altering the expression of cathepsin B, tumor suppressor genes and autophagy-related proteins. *Front Bioeng Biotechnol*. 2020;8:601969. doi:10.3389/fbioe.2020.601969
24. Feng F, Pan L, Wu J, et al. Cepharanthine inhibits hepatocellular carcinoma cell growth and proliferation by regulating amino acid metabolism and suppresses tumorigenesis in vivo. *Int J Biol Sci*. 2021;17(15):4340–4352. doi:10.7150/ijbs.64675
25. Wonbong L, Gayoung J, Young Lee B, Ho Park M, Hyun H. Rapid clearance of IR783 and methyl-β-cyclodextrin complex for improved tumor imaging. *Part Syst Charact*. 2021;38:2100068. doi:10.1002/ppsc.202100068
26. Chou T-C. Theoretical basis, experimental design, and computerized simulation of synergism and antagonism in drug combination studies. *Pharmacol Rev*. 2006;58(3):621–681. doi:10.1124/pr.58.3.10
27. Chou TC, Talalay P. Quantitative analysis of dose-effect relationships: the combined effects of multiple drugs or enzyme inhibitors. *Adv Enzyme Regul*. 1984;22:27–55. doi:10.1016/0065-2571(84)90007-4
28. Chou T-C. Drug combination studies and their synergy quantification using the Chou-Talalay method. *Cancer Res*. 2010;70(2):440–446. doi:10.1158/0008-5472.CAN-09-1947
29. Houdaihed L, Evans JC, Allen C. Codelivery of paclitaxel and everolimus at the optimal synergistic ratio: a promising solution for the treatment of breast cancer. *Mol Pharmaceut*. 2018;15(9):3672–3681. doi:10.1021/acs.molpharmaceut.8b00217
30. Hidalgo M, Sánchez-Moreno C, de Pascual-Teresa S. Flavonoid–flavonoid interaction and its effect on their antioxidant activity. *Food Chem*. 2010;121(3):691–696. doi:10.1016/j.foodchem.2009.12.097
31. Tardi P, Johnstone S, Harasym N, et al. In vivo maintenance of synergistic cytarabine: Daunorubicin ratios greatly enhances therapeutic efficacy. *Leukemia Res*. 2009;33(1):129–139. doi:10.1016/j.leukres.2008.06.028
32. Tardi PG, Dos Santos N, Harasym TO, et al. Drug ratio–dependent antitumor activity of irinotecan and cisplatin combinations in vitro and in vivo. *Mol Cancer Ther*. 2009;8(8):2266–2275. doi:10.1158/1535-7163.MCT-09-0243
33. Li L, He D, Guo Q, et al. Exosome-liposome hybrid nanoparticle codelivery of TP and miR497 conspicuously overcomes chemoresistant ovarian cancer. *J Nanobiotechnol*. 2022;20:1. doi:10.1186/s12951-021-01184-w
34. Jain RK, Stylianopoulos T. Delivering nanomedicine to solid tumors. *Nat Rev Clin Oncol*. 2010;7(11):653–664. doi:10.1038/nrclinonc.2010.139
35. Fan L, Du P, Li Y, et al. Targeted liposomes sensitize plastic melanoma to ferroptosis via senescence induction and coenzyme depletion. *ACS Nano*. 2024;18(9):7011–7023. doi:10.1021/acsnano.3c10142
36. Large DE, Abdelmessih RG, Fink EA, Auguste DT. Liposome composition in drug delivery design, synthesis, characterization, and clinical application. *Adv. Drug Delivery Rev*. 2021;176. doi:10.1016/j.addr.2021.113851
37. Antoniou AI, Giofrè S, Seneci P, Passarella D, Pellegrino S. Stimulus-responsive liposomes for biomedical applications. *Drug Discovery Today*. 2021;26(8):1794–1824. doi:10.1016/j.drudis.2021.05.010
38. Kapoor M, Lee SL, Tyner KM. Liposomal drug product development and quality: current US experience and perspective. *AAPS J*. 2017;19(3):632–641. doi:10.1208/s12248-017-0049-9
39. Seubwai W, Vaeteewoottacharn K, Hiyoshi M, et al. Cepharanthine exerts antitumor activity on cholangiocarcinoma by inhibiting NF-kappaB. *Cancer Sci*. 2010;101(7):1590–1595. doi:10.1111/j.1349-7006.2010.01572.x
40. Xu W, Chen S, Wang X, Wu H, Yamada H, Hirano T. Bisbenzylisoquinoline alkaloids and P-glycoprotein function: a structure activity relationship study. *Bioorg Med Chem*. 2020;28(12):115553. doi:10.1016/j.bmc.2020.115553
41. Ayllon M, Abatchev G, Bogard A, Whiting R, Hobdey SE, Fologea D. Liposomes prevent in vitro hemolysis induced by streptolysin O and lysenin. *Membranes*. 2021;11:5.
42. Zou Y, Huang D, He S, et al. Cooperatively enhanced photothermal-chemotherapy via simultaneously downregulating HSPs and promoting DNA alkylation in cancer cells. *Chem. Sci.* 2023;14(4):1010–1017. doi:10.1039/D2SC06143K
43. Nam J, Son S, Ochyl LJ, Kuai R, Schwendeman A, Moon JJ. Chemo-photothermal therapy combination elicits anti-tumor immunity against advanced metastatic cancer. *Nat Commun*. 2018;9:1. doi:10.1038/s41467-018-03473-9
44. Yin X, Fan T, Zheng N, et al. Palladium nanoparticle based smart hydrogels for NIR light-triggered photothermal/photodynamic therapy and drug release with wound healing capability. *Nanoscale Adv*. 2023;5(6):1729–1739. doi:10.1039/D2NA00897A
45. Hu Y, Zhang L, Chen S, et al. Multifunctional carbon dots with near-infrared absorption and emission for targeted delivery of anticancer drugs, tumor tissue imaging and chemo/photothermal synergistic therapy. *Nanoscale Adv*. 2021;3(24):6869–6875. doi:10.1039/D1NA00595B
46. Celikbas E, Saymaz A, Gunduz H, et al. Image-guided enhanced PDT/PTT combination therapy using brominated hemicyanine-loaded folate receptor-targeting Ag2S quantum dots. *Bioconjugate Chem*. 2023;34(5):880–892. doi:10.1021/acs.bioconjchem.3c00096